PROCEEDINGS OF THE 2ND NORTH AMERICAN ROCK MECHANICS SYMPOSIUM: NARMS'96
A REGIONAL CONFERENCE OF ISRM/MONTRÉAL/QUÉBEC/CANADA/19-21 JUNE 1996

Rock Mechanics Tools and Techniques

Edited by

MICHEL AUBERTIN
Ecole Polytechnique, Montréal, Québec, Canada

FERRI HASSANI
McGill University, Montréal, Québec, Canada

HANI MITRI
McGill University, Montréal, Québec, Canada

A.A. BALKEMA/ROTTERDAM/BROOKFIELD/1996.

Rock Mechanics, Aubertin, Hassani & Mitri (eds) © 1996 Balkema, Rotterdam. ISBN 90 54 10 838 X

Three dimensional finite element simulations of room and pillar mines in rock salt

Edward L. Hoffman & Brian L. Ehgartner
Sandia National Laboratories, Albuquerque, h! Mex., USA

ABSTRACT: Three-dimensional quasistatic finite element codes are being used at Sandia National Laboratories to simulate large room and pillar mines in rock salt. Two simulations are presented: a one-level salt production mine and a much larger two-level salt production mine. These calculations, based on actual mines, apply Sandia-developed technology to the solution of problems which were previously not solvable. These simulations. validated by field measurements and observations, have provided valuable insight into the failure mechanisms of room and pillar mines in rock salt. Although the simulations were performed in the interest of Sandia's programs, these results should be of general interest to mine operators.

1 INTRODUCTION

The ability to predict the mechanical response of rock salt in three dimensions (3D) to the excavation and operation of large room and pillar mines would potentially give mine operators the capability of designing safer and more efficient mines. Room and pillar mines typically consist of several hundred pillars. Because each pillar needs sufficient mesh refinement to capture the deformation modes, finite element models of room and pillar mines may require several hundred thousand elements. Currently available commercial finite element technology does not treat geometric and material nonlinearities efficiently enough to handle problems of this size. Because of the solution techniques and constitutive models used in commercial finite element technology, practical limits of around ten thousand elements are typical. As a result, these complex structures are typically simplified into 2D plane strain models or 3D models of a single pillar. The latter quasi-3D models simulate a mine consisting of an infinite number of rooms and pillars. Neither of these simplified models accurately describe the complex 3D mechanics of a room and pillar mine.

Sandia has a long history of research and development in nonlinear large strain finite element codes and the application of these codes to geomechanics problems in waste management programs. Sandia's quasistatic finite element technology is based on iterative solvers and has been extensively developed for large problems involving nonlinear large deformations. The use of iterative solvers and experience with nonlinear material response provided the required technology to solve these large, complex problems. The finite element code used to perform the calculations presented in this paper, JAC3D (Biffle 1992), uses an eight-node hexahedral Lagrangian uniform strain element with hourglass stiffness to control zero energy modes. A nonlinear conjugate gradient method is used to solve the nonlinear system of equations. For nonlinear problems, this efficient solution scheme is considerably faster than the direct solvers which are used in most commercial codes.

Two simulations are presented in this paper: a relatively small one-level salt production mine and a much larger two-level salt production mine converted for liquid storage. These examples, based on actual mines, presented an excellent opportunity to apply Sandia technology to the solution of a problem class which was previously not solvable. The simulations were used to investigate the effect of pillar slabbing on mine stability, and the development of a disturbed rock zone due to mine excavation and its effect on the hydrological integrity of the mine. Much has been learned from the use of full 3D models that was not known when 2D and quasi-3D models were in use. Although this work was performed to address issues of specific interest to Sandia programs, these calculations have identified performance issues which should be of general interest to mine operators.

2 MATERIAL MODELS

The two examples presented in this paper are based on mines excavated in salt domes. The stratigraphy overlying the massive salt formation, known as the overburden. consists of sand and gravel mixed with clay and silt. The ground water regime in these highly permeable sediments is a single aquifer which extends from just below the surface (at sea level) to the top of the salt. Salt in its natural state is typically considered impermeable. Hence, it provides an excellent barrier between a mine and the overlying groundwater. In the event that a leak developed through the salt into the underground workings, the initial inflow would be saturated. However, if sufficiently high flow rates are established, then flow from less saline portions of the water table could enter the mine causing the solution rate to increase and possibly resulting in flooding of the mine. Hence, in order to assess the stability of the mines, it was important to have the host salt well characterized, both structurally and hydrologically. The constitutive and failure models used in these calculations are presented in the following sections.

2.1 Constitutive models

The sandy overburden was modeled as an elastic material in the following calculations. However, salt exhibits both elastic and creep behavior. Based on the secondary creep model used in these calculations (Krieg 1984). the creep strain rate is a function of the equivalent deviatoric stress and is expressed as follows:

$$\dot{\bar{\varepsilon}}^{cr} = A\bar{\sigma}^{n}\exp\left(-\frac{Q}{RT}\right) \qquad (2.1)$$

where

$\dot{\bar{\varepsilon}}^{cr}$ is the creep strain rate,

$\bar{\sigma}$ is the effective or von Mises stress,

T is absolute temperature,

A and n are constants determined from fitting the model to creep data,

Q is the effective activation energy (cal/mole),

R is the universal gas constant (1.987 cal/mole-K).

The properties used for the overburden and salt are reported in Table 1.

2.2 Structural stability criteria for rock salt

In this paper, the structural stability of rock salt is evaluated based on two failure criteria: dilatant damage and tensile failure. The dilatant damage criterion, developed from laboratory data, is used to delineate potential zones of dilatancy in the salt formation surrounding an underground excavation. Dilatancy is attributed to microfracturing or changes in the pore structure of the salt, resulting in an increase in permeability and, hence, a flow path for groundwater. The dilatancy surface (Van Sambeek 1993) is defined by a "damage" factor, quantifying the potential for dilatant behavior, expressed as $D = \sqrt{J_2}/(0.25\ I_1)$. where J_2 is the second invariant of the deviatoric stress tensor, and I_1 is the first invariant of the stress tensor. When D is equal to or greater than one, the shear stresses in the salt are large compared to the mean stress and dilatant behavior is expected. The region of salt which experiences a change in its pore structure due to the excavation of underground openings has become known as the disturbed rock zone (DRZ).

Rock salt typically has a very low tensile strength (approximately I MPa). For the purposes of these analyses, the tensile strength of salt was assumed to be zero. Tensile cracking in rock salt tends to initiate perpendicular to the largest tensile stress in the rock sample. The largest tensile stress is one of the *principal stresses.* Because the maximum principal stress is the algebraically largest of the three principal stresses (in 3D space) and the largest normal stress in any direction, the potential for tensile failure exists if the maximum principal stress is tensile.

Table 1: Structural properties of overburden and salt.

	Elastic Properties			Creep Properties		
Material	Young's Modulus, E (GPa)	Poisson's Ratio, ν	Density, ρ (kg/m^3)	A (Pa$^{-4.9}$/sec)	n	Activation Energy, Q (kcal/mole)
Salt	31.0	0.250	2300	5.79×10^{-36}	4.90	12.0
Overburden	0.1	0.330	1874	--	--	--

3 ONE-LEVEL MINE SIMULATION

The one-level mine simulation presented in this section is based on an actual salt production mine. The mine is relatively small as it was only active for less than two years. The model, though not an exact representation, captures the relevant parameters of the mine (depth, extraction ratio, etc.). A major concern regarding the stability of this mine was the extensive spalling of salt slabs from pillar walls. Slabs approximately 3 m-thick were reported to have spalled, yielding an hourglass shaped pillar as shown in Figure 1. The majority of this slabbing occurred in the first few years of operation. Later reports indicated that there had been little or no change in the condition of the mine in subsequent years. The primary concern was what effect, if any, would this spalling have on pillar and mine stability.

3.1 Geomechanical model

The finite element model of the one-level mine is shown in Figure 2. The quarter symmetry model, consisting of 84,968 nodes and 78,720 elements, idealizes a 45 pillar (5 by 9) mine. The mine consists of a region of 27.4 m-high rooms called the benched area and a perimeter area of 7.62 m-high rooms called the unbenched area, The roof elevations of the benched and unbenched portions of the mine are the same. The pillars are 29 m-square and the rooms are

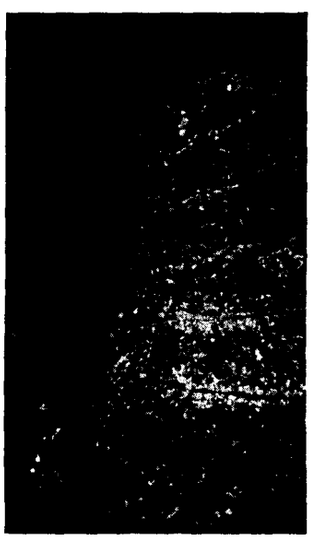

Figure 1. Photograph of a spalling pillar.

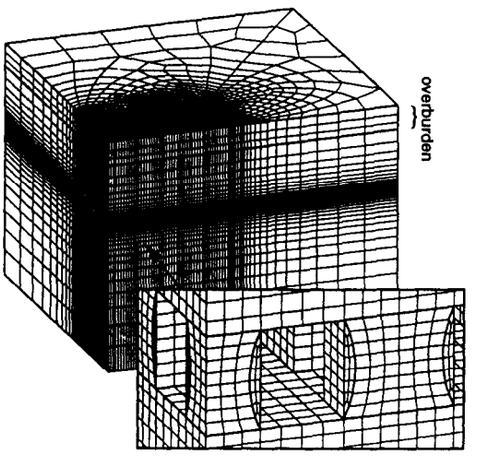

Figure 2. Finite element model of the one-level mine

22.9 m-wide in both the benched and unbenched areas, resulting in an extraction ratio of 0.69. The extraction ratio is defined as the room area, measured in a horizontal plane, divided by the total area (including room and pillar). The simulations assume instantaneous formation of the mine which is appropriate as the mine was excavated in a relatively short period of time.

Gravitational body forces are applied to the model. To ensure initial equilibrium, elevation-dependent initial stresses are applied to each element in the model. The vertical stress component is based on the weight of the overbearing material (using the properties given in Table 1). For the salt, an initial stress state is assumed in which the horizontal stress component is equal to the vertical stress component (lithostatic). For the overburden, the horizontal component is applied to be consistent with a vertically loaded elastic material in equilibrium. Under these load conditions, the resulting ratio of horizontal to vertical stress is defined as $\nu/(1-\nu)$, where ν is the Poisson's ratio of the material. Displacements are constrained normal to all four vertical boundaries and the lower horizontal boundary.

The finite element model includes a depth-dependent temperature gradient which starts at 26.8' C at the surface and increases at the rate of 0.0222' C/m. The temperature distribution is important because the creep response of the salt is temperature dependent. One-way thermal coupling was assumed by entering the thermal data into the structural calculations. This assumption was appropriate since the deformations were not large enough to significantly affect the ther-

mal analysis. Surface cooling (due to ventilation) was assumed to have a negligible effect on salt temperature and consequent deformation rates.

The progressive pillar failure observed in the mine was modeled by computationally removing salt from initially square pillars to form hourglass-shaped pillars similar to those. observed in the mine. Although this model does not simulate the failure mechanisms which lead to spalling, it is useful to determine the post-spalled stress state of the pillars and to evaluate the stability of the pillars after spalling. The calculations presented in this paper are based on the approximate history of the mine. The first hvo years of the simulation. the pillars are intact. At two years, the spalled material regions were removed using the element death option in JAC3D. The simulations were extended another sixteen years following spalling.

3.2 Results of the one-level mine simulations

Figure 3 shows a contour plot of maximum principal stress in the one-level mine before spalling, immediately after spalling, and 16 years after spalling. Prior to spalling, a region of tensile stress develops which is approximately 3 m thick at the pillar mid-height. After this region of material is removed, the stress distribution in the pillar changes such that there are no tensile stresses in the pillar. This is due to the fact that the hourglass shape places the pillar in confinement. Sixteen years after spalling, the maximum principal stresses in the pillars remain compressive. These results suggest that spalling is initiated early in the life of the mine by the development of tensile stress in the pillar. The post-spalling shape of the pillar results in the redistribution of stresses such that no further failure will occur as a result of tensile stress, indicating that the mine is stable with respect to this failure mechanism. This would explain why the very little slabbing was observed in the mine after the early failures. The simulations also predict the development of high tensile stresses in the floor of the unbenched perimeter. Fracturing and floor heave have been observed in these locations of the mine.

Contour plots of dilatant damage are shown in Figure 4 before spalling, immediately after spalling, and 16 years after spalling. The criterion is plotted only for the salt and not the overburden since the criterion was developed specifically for rock salt. Dilatant damage is indicated where D > 1.0. Before spalling. the DRZ is confined to a small region surrounding the mine. After spalling, the DRZ has increased in size, but the magnitude of damage in the pillars is significantly reduced. Again, this suggests

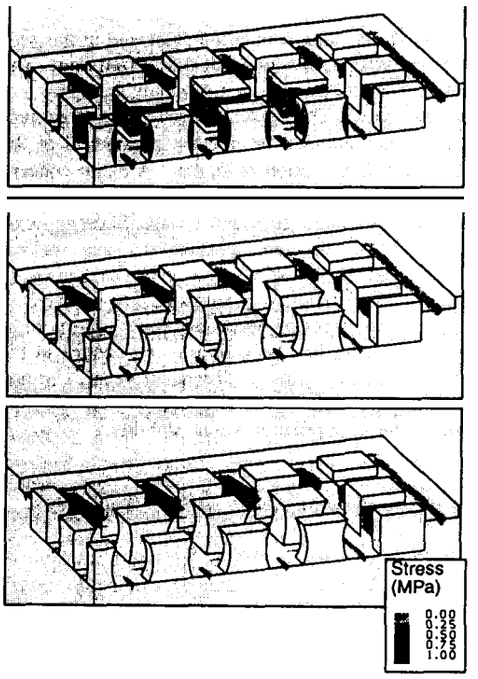

Figure 3. Maximum principal stress distribution in the one-level mine before spalling, immediately after spalling, and 16 years after spalling.

that spalling results in a stress redistribution which is more stable. The spalling results in a slight increase in the damage factor directly above the mine at the overburden/salt interface. However, the damage factor is still less than one. Sixteen years after spalling, a DRZ begins to appear over one of the mine boundaries at the overburden/salt interface. Furthermore, the DRZ surrounding the mine begins to extend upward at this same boundary. However, the DRZ is small and should not effect the hydrological integrity of the mine. These predictions are supported by the fact that, at present, this mine has experienced no significant influx of water.

4 TWO-LEVEL MINE SIMULATION

The two-level room and pillar mine simulation presented in this section is based on an actual salt production mine. After the mine was completed, it was converted for liquid storage. The mine has two types of boundaries: stepped boundaries, where the lower

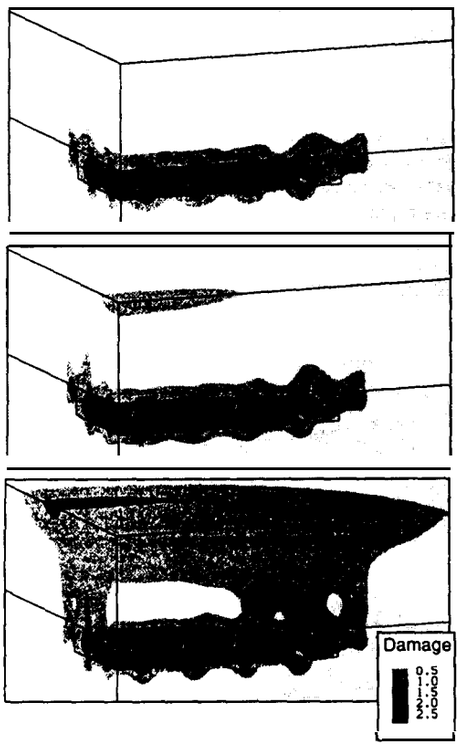

Figure 4. Dilatant damage distribution in the one-level mine before spalling, immediately after spalling, and 16 years after spalling.

level extends beyond the upper level, and unstepped boundaries, where the extent of the upper and lower levels is the same. A sinkhole was recently discovered on the surface, above one of the *mine* boundaries. The discovery suggested that the mine may be experiencing inflows from the aquifer located above the salt dome. The following calculations will show the probable cause of the sinkhole. Although the mine is not accessible for observation, surface subsidence data is available for comparison with the numerical model.

4.1 Geomechanical model

The finite element model of the two-level room and pillar mine is shown in Figure 5. The quarter symmetry model contains 201,237 nodes and 189,700 elements, representing one of the largest calculations performed with JAC3D to date. The model simulates

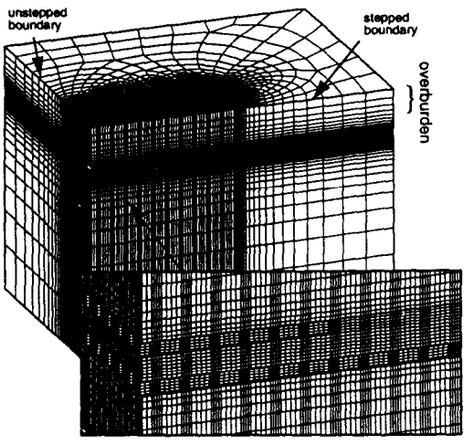

Figure 5. Finite element model of the two-level mine

a 340 pillar mine which is stepped on two opposite sides and unstepped on the other two sides. Although it is not an exact representation of the mine, the model captures the most relevant geometrical parameters (e.g. mine depth, extraction ratio, room height. etc.). The upper and lower levels of the mine are located 163 m and 224 m below the surface, respectively (measured to the floor of the mine). The pillars are 30.5 m-square and the rooms are 15.2 m-wide, resulting in an extraction ratio of 56 percent. The lower level pillars were laid out directly under the upper level pillars. Hence, the room and pillar dimensions of the lower level repeat those of the upper level. The room height is 22.9 m for both levels.

Displacements are constrained normal to all four vertical boundaries and the lower horizontal boundary. Gravity loads, initial stresses, and imposed thermal conditions are applied to the model just as those described for the one-level mine.

The calculations simulate the approximate history of the mine which is presented in Table 2. The excavation times assume instantaneous formation of the upper and lower levels. In reality, the mines were formed over a long period of time. The excavation

Table 2: History of the two-level mine.

Analysis Time (years)	Event
0	Excavate upper level
38	Excavate lower level
51	Liquid fill
79	Terminate simulation

times for instantaneous formation are the average mining dates. The simulation begins with the excavation of the upper level. To simulate the excavation of the lower level, the elements filling the lower level were removed using the element death option in JAC3D. Finally, a depth dependent pressure distribution simulating liquid till (specific gravity of 0.86) is applied to the lining of the mine. The calculation was terminated 79 years into the simulation.

4.2 Results of the two-level mine simulations

It is desirable, whenever possible, to compare simulations with field data. A comparison of subsidence rate measurements over the actual mine to the predicted subsidence profile is presented in Figure 6. The subsidence data are corrected such that the farfield subsidence rates are identically zero. The model definition of surface position (s) was selected such that it first crosses an unstepped boundary and then the stepped boundary. This is similar to the path of the field data which first crosses an unstepped boundary and then a stepped boundary. The calculations show reasonably good agreement with the field data considering the approximate nature of the model (e.g. instantaneous excavation, pillar spalling not modeled, etc.). Although the magnitude of the subsidence rates differ, the basic shape of the subsidence trough agrees for both the model and field measurements. The extent or width of the subsidence agrees very closely, validating the model prediction that subsidence is localized to within a small range of the mine boundary. Furthermore, the data confirms that the slope of the subsidence contour is steeper where the mine is not stepped, causing a smaller radius of curvature of the subsidence profile and, hence, greater bending of the overlying salt and overburden.

The dilatant damage factor is plotted in Figure 7 for simulation times of 38, 51, 67, and 79 years. The first two times correspond to excavation of the lower level and liquid fill, respectively. The third time corresponds approximately to the present time. Like the one-level mine, a DRZ develops in the walls, floor and ceiling of the mine. However, unlike the one-

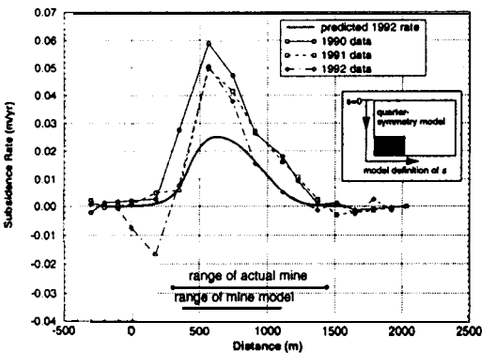

Figure 6. Comparison of predicted subsidence rates to field data.

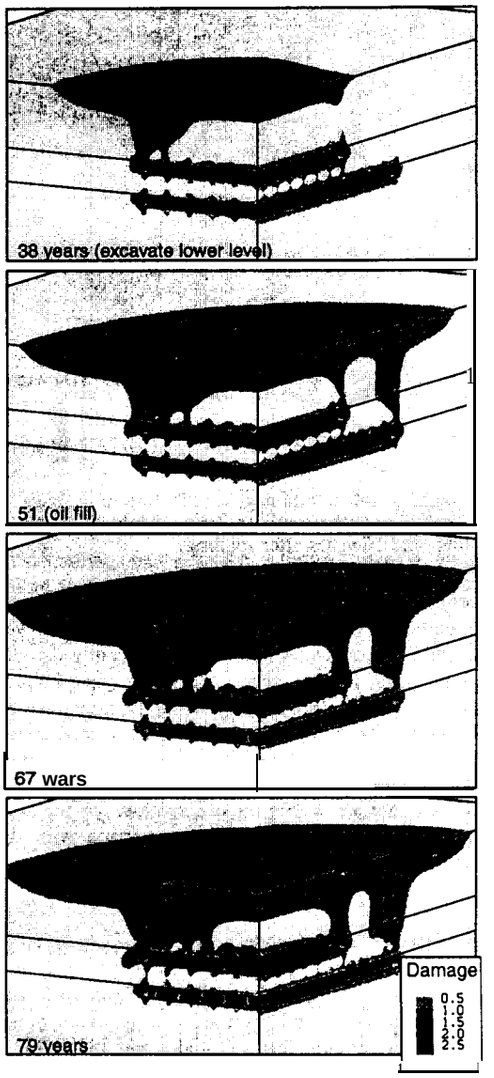

Figure 7. Dilatant damage distribution around the two-level mine.

level mine, the two-level mine simulations predict the development of a DRZ initiating at the salt/overburden interface, directly over the unstepped boundary. This DRZ initiates when the lower level of the mine is excavated. The DRZ grows with time, extending toward the comer of the mine. The growth rate is highest during the time period between lower level excavation and liquid fill. Nearly 30 years after lower level excavation, the DRZ is predicted to have progressed more than half-way through the salt roof. By the end of the simulation, the DRZ has grown even larger and is within 25 m of the DRZ developing around the mine. The DRZ is largest over the unstepped boundary due to the greater bending at this location, indicated by the steeper subsidence trough over this boundary (see Figure 6). This corresponds to the location where the sinkhole developed. The development of the sinkhole is indicative that the DRZ may have connected the mine to the overlying aquifer. It should be noted that, because the sinkhole developed along the boundary of the facility, this mode of mine failure could only be identified with a full 3D model of the mine, including both stepped and unstepped boundaries.

This predicted DRZ around the mine boundary may have been encountered while mining a drift from one of the shafts of this two-level mine. A zone of wet salt was encountered during routine drilling and blasting. Mining was halted and, after significant brine inflows, a bulkhead was installed at the entrance of the drift. The drift is located along one of the unstepped boundaries of the mine. Hence, this region of wet salt may be attributed to dilatant damage caused by the two-level excavation.

5 SUMMARY AND CONCLUSIONS

Two complex room and pillar mines were analyzed with JAC3D, a three-dimensional quasistatic finite element code developed at Sandia National Laboratories. The iterative methods and reduced integration techniques used in JAC3D are considerably faster and use significantly less memory than the direct solvers used in most commercial finite element codes. The economical solution of these problems indicates that iterative techniques are powerful tools for the analysis of large multi-level mines. In fact. these may be the only tools capable of solving problems of this size.

These simulations, validated by field measurements and observations, have provided better insight into the failure mechanisms of room and pillar mines in rock salt. Pillar spalling was commonly thought to be a degenerative process which would progress until the pillar ultimately failed. The pillar spalling simulations identified tensile failure as the probable cause of pillar spalling. The calculations demonstrate that spalling produces a pillar shape which has a stable stress distribution. Most importantly, the calculations demonstrate that the spalling process has no observed effect on the overall stability or hydrological integrity of the mine. The simulations of the two level mine demonstrate a possible failure mechanism which may have led to a leak into the mine. These calculations demonstrate that the size of the DRZ is dependent upon the geometrical configuration of the mine. The DRZ did not develop until the lower level of the mine was excavated. Furthermore, the magnitude and extent of the DRZ was significantly larger over the unstepped boundaries. Although these simulations were performed in the interest of Sandia programs, these results should be of general interest to mine operators.

Acknowledgements-This work was supported by the United States Department of Energy (DOE) under contract No. DE-AC04-76DP00789.

REFERENCES

Biffle, J.H. 1992. ***JAC3D - A three-dimensionalfinite element computer program for the nonlinear quasistatic response of solids with the conjugate gradient method*** SAND87-1305. Sandia National Laboratories, Albq., NM.

Krieg, R.D. ***Reference stratigraphy and rock properties of the Waste Isolation Pilot Plant (WIPP) project*** SAND83-1908. Sandia National Laboratories, Albq., NM.

Van Sambeek, L.L., J.L. Ratigan, & ED. Hansen 1993. Dilatancy of rock salt in laboratory tests. ***Proc. 34th U.S. Symposium on Rock Mechanics.***